Nanoscale

Accepted Manuscript

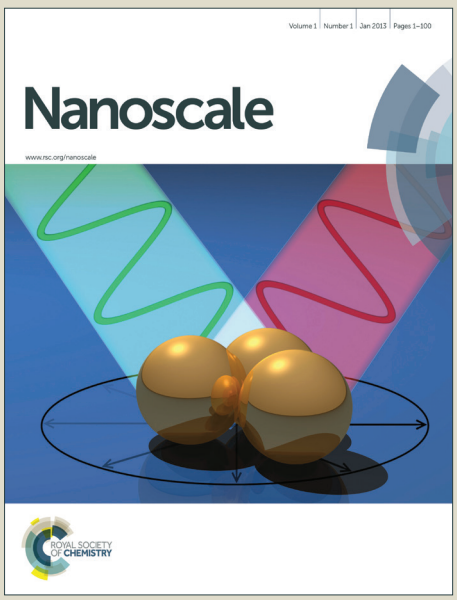

ROYAL SOCIETY OF CHEMISTRY

www.rsc.org/nanoscale

Cite this: DOI: 10.1039/c0xx00000x

www.rsc.org/xxxxxx

PAPER

RGD-functionalized ultrasmall iron oxide nanoparticles for targeted T_1-weighted MR imaging of glioma†

Yu Luo,[1a] Jia Yang,[1b] Yu Yan,[a] Jingchao Li,[a] Mingwu Shen,*[a] Guixiang Zhang,*[b] Serge Mignani[c] and Xiangyang Shi*[a]

Received (in XXX, XXX) Xth XXXXXXXXX 20XX, Accepted Xth XXXXXXXXX 20XX
DOI: 10.1039/b000000x

We report a convenient approach to preparing ultrasmall Fe_3O_4 nanoparticles (NPs) functionalized with arginylglycylaspartic acid (RGD) peptide for *in vitro* and *in vivo* magnetic resonance (MR) imaging of glioma. In our work, stable sodium citrate-stabilized Fe_3O_4 NPs were prepared by a solvothermal route. Then, the carboxylated Fe_3O_4 NPs stabilized with sodium citrate was conjugated with polyethylene glycol (PEG)-linked RGD. The formed ultrasmall RGD-functionalized nanoprobe (Fe_3O_4-PEG-RGD) was fully characterized using different techniques. We show that these Fe_3O_4-PEG-RGD particles with a size of 2.7 nm are water-dispersible, stable, cytocompatible and hemocompatible in a given concentration range, and display targeting specificity to glioma cells overexpressing $\alpha_v\beta_3$ integrin *in vitro*. With the relatively high r_1 relaxivity (r_1 = 1.4 $mM^{-1}s^{-1}$), the Fe_3O_4-PEG-RGD particles can be used as an efficient nanoprobe for targeted T_1-weighted positive MR imaging of glioma cells *in vitro* and the xenografted tumor model *in vivo via* an active RGD-mediated targeting pathway. The developed RGD-functionalized Fe_3O_4 NPs may hold great promise to be used as a nanoprobe for targeted T_1-weighted MR imaging of different $\alpha_v\beta_3$ integrin-overexpressing cancer cells or biological systems.

Introduction

Among the various molecular imaging techniques, magnetic resonance (MR) imaging has been identified as one of the most powerful noninvasive imaging techniques due to its high spatial resolution and tomographic capabilities, and the ability to acquire three-dimensional (3D) tomographic information of tissues with high soft tissue contrast.[1-4] However, for highly-sensitive and accurate MR imaging applications, enhanced contrast between normal and pathological tissues is required. Consequently, the use of exogenous MR contrast agents is crucial.

Currently, most of the MR positive contrast agents are either paramagnetic Gd or Mn chelate-based agents. Nevertheless, the recently reported nephrogenic system fibrosis associated with Gd(III)-based contrast agents caused serious safety concerns, especially in patients with abnormal kidney function.[5-8] Accordingly, development of new stable biocompatible positive MR contrast agents still remains a great challenge.

In an earlier work, Roca and coworkers have shown that the magnetic property of Fe_3O_4 nanoparticles (NPs) is strongly dependent on their sizes.[9] The magnetic moment of Fe_3O_4 NPs reduces sharply as their size decreases due to the reduction of their volume magnetic anisotropy and spin disorders on the surface of the NPs, thus inhibiting the T_2 effect and conversely maximizing the T_1 contrast effect.[10, 11] Therefore, small sized Fe_3O_4 NPs (< 5 nm) have been used as T_1 contrast agents for MR imaging applications.[12, 13]

Thermal decomposition of iron precursors in nonpolar organic solvents has been employed to produce extremely small-sized iron oxide NPs (diameter ~ 5 nm).[14-16] Nonetheless, this approach suffers several drawbacks: 1) the formed Fe_3O_4 NPs are water insoluble due to their coated hydrophobic ligands, limiting their biomedical uses;[17, 18] 2) in most of these studies related to cancer diagnosis, a passive targeting strategy, based on the well-known enhanced permeability and retention (EPR) effect, has been adopted to image the tumor tissues with leaky vasculature and poor lymphatic drainage. Consequently, for efficient and specific MR imaging of tumors, it is essential to modify the NPs with various targeting ligands that can direct the particles specifically to the tumor region *via* a receptor-mediated active targeting strategy.[19-22] Another approach is to prepare water-dispersible ultrasmall Fe_3O_4 NPs using sodium citrate as a stabilizer *via* a facile one-pot solvothermal route.[23] Unfortunately, the formed citrate-stabilized ultrasmall Fe_3O_4 NPs have not been functionalized to have targeting specificity for targeted T_1-weighted MR imaging of tumors.

Polymer grafting has been considered to be one of the most effective approaches used for NP surface functionalization.[24-26] In our previous work, we have shown that polyethyleneimine (PEI)-coated Fe_3O_4 NPs formed *via* a one-step hydrothermal approach can be modified by polyethylene glycol (PEG) to render the particles with minimum macrophage cellular uptake,[27] be functionalized with targeting ligands such as folic acid (FA)[28] or hyaluronic acid[29] for targeted T_2-weighted negative MR imaging

of tumors overexpressing FA receptors or CD44 receptors, respectively. In addition, PEI-coated Fe_3O_4 NPs formed *via* a mild reduction can also be functionalized with FA[30] or arginylglycylaspartic acid (RGD) peptide[31] *via* a PEG spacer for targeted T_2-weighted negative MR imaging of specific tumors. Meanwhile, preformed Fe_3O_4 NPs can also be assembled with functionalized dendrimers for T_2-weighted negative MR imaging applications.[32, 33] These strategies may be used to functionalize citrate-stabilized ultrasmall Fe_3O_4 NPs for targeted T_1-weighted MR imaging of tumors. In our recent attempt, we have shown that citrate-stabilized ultrasmall Fe_3O_4 NPs can be assembled onto generation 5 RGD-functionalized dendrimers.[34] However, due to the formation of the clustered particles, the prepared dendrimer-functionalized Fe_3O_4 NPs can only be used for T_2-weighted negative MR imaging of $\alpha_v\beta_3$ integrin-overexpressing tumors.

In this present study, we report a convenient approach to forming RGD-functionalized ultrasmall Fe_3O_4 NPs for targeted T_1-weighted positive MR imaging of glioma overexpressing $\alpha_v\beta_3$ integrin. In our approach, stable sodium citrate-stabilized Fe_3O_4 NPs prepared by a solvothermal route were conjugated with PEGylated RGD *via* 1-ethyl-3-(3-dimethylaminopropyl) carbodiimide hydrochloride (EDC) chemistry (Figure 1). The formed Fe_3O_4-PEG-RGD NPs were fully characterized. The cytocompatibility and hemocompatibility of the NPs were evaluated by cell viability and hemolysis assays, respectively. The RGD-mediated targeting of the Fe_3O_4-PEG-RGD NPs towards U87MG cells (a human glioma cell line) overexpressing high-affinity $\alpha_v\beta_3$ integrin was confirmed by both ICP-AES analysis and Prussian blue staining. Finally, the feasibility to use the developed NPs as a nanoprobe for targeted T_1-positive MR imaging of cancer cells *in vitro* and the xenografted tumor model *in vivo* was also explored. To our knowledge, this is the first report related to the use of ultrasmall Fe_3O_4 NPs functionalized with targeting ligands for specific T_1-positive MR imaging of tumors.

Experimental

Materials

Diethylene glycol, EDC, and *N*-hydroxysuccinimide (NHS) were purchased from Aldrich (St Louis, MO). RGD was from GL Biochem (Shanghai, China). A dual functional PEG with one end of amine group and the other end of maleimide group (NH_2-PEG_{2000}-Mal, Mw = 2,000) and PEG monomethyl ether with the other end of amine group (*m*PEG-NH_2, Mw = 2,000) were purchased from Shanghai Yanyi Biotechnology Corporation (Shanghai, China). U87MG cells (a human glioma cell line) and L929 cells (a mouse fibroblast cell line) were obtained from Institute of Biochemistry and Cell Biology (the Chinese Academy of Sciences, Shanghai, China). Dulbecco's Modified Eagle Medium (DMEM), fetal bovine serum (FBS), penicillin, and streptomycin were purchased from Gibco (Carlsbad, CA). Sodium citrate, anhydrous ferric chloride ($FeCl_3$ > 99%) and all other chemicals were from Sinopharm Chemical Reagent Co., Ltd (Shanghai, China) and used as received. Water used in all experiments was purified using a Milli-Q Plus 185 water purification system (Millipore, Bedford, MA) with a resistivity higher than 18 MΩ.cm. Regenerated cellulose dialysis membranes (molecular weight cut-off, MWCO = 10,000) were acquired from Fisher Scientific (Pittsburgh, PA).

Synthesis of the Fe_3O_4-PEG-RGD NPs

Synthesis of citrate-stabilized Fe_3O_4 NPs. $FeCl_3.6H_2O$ (1081 mg) was dissolved in 40 mL of diethylene glycol under stirring to form a homogeneous solution. Sodium citrate (471 mg) was added to the above solution, and the mixture was heated to 80 °C in a water bath until a clear solution was formed. Subsequently, sodium acetate (1312 mg) was added to the above mixture solution and dissolved, and then the mixture was transferred to a Teflon-lined stainless-steel autoclave with a volume of 100 mL and sealed in air. The autoclave was placed into an oven at 200 °C for 4 h. After cooling down to room temperature, the black solution was collected by centrifugation (10000 rpm, 5 min) and purified with ethanol for 3 times to remove excess reactants and byproducts. The resulting black product was redispersed into water and lyophilized to obtain the powder of the Fe_3O_4 NPs for further use.

Synthesis of NH_2-PEG-RGD. NH_2-PEG-Mal (20.00 mg) was dissolved in 5 mL DMSO under vigorous magnetic stirring at room temperature, followed by addition of RGD (6.92 mg, 2 mL in DMSO). The reaction mixture was stirred for 24 h. After that, the mixture was subjected to dialysis against phosphate buffered saline (PBS, 3 times, 2 L) and water (6 times, 2 L) for 3 days using a dialysis membrane with an MWCO of 1,000 to remove the DMSO and the excess of reactants and byproducts. A further lyophilization step gave rise to the product of NH_2-PEG-RGD in a white powder.

Preparation of the Fe_3O_4-PEG-RGD NPs. The citric acid carboxyl group of Fe_3O_4 NPs (56 mg, in 10 mL DMSO) was first activated with EDC (144 mg, dissolved in 1 mL DMSO) and NHS (70 mg, dissolved 1 mL DMSO) at room temperature for 3 h. Then, the resulting solution was dropwise added into a DMSO solution of NH_2-PEG-RGD (11.08 mg, 5 mL) under vigorous stirring at room temperature for 3 days. Finally, the reaction mixture was dialyzed against PBS (3 times, 2 L) and water (6 times, 2 L) for 3 days using a dialysis membrane with an MWCO of 3,000, followed by lyophilization to obtain the product of the Fe_3O_4-PEG-RGD NPs (Figure 1). For comparison, Fe_3O_4 NPs were also reacted with *m*PEG-NH_2 under similar experimental conditions to afford the formation of the Fe_3O_4-*m*PEG NPs.

Characterization techniques

^{1}H NMR spectra were collected using a Bruker AV400 nuclear magnetic resonance spectrometer. Samples were dissolved in D_2O before measurements. Thermogravimetric analysis (TGA) was carried out using a TG 209 F1 (NETZSCH Instruments Co., Ltd., Bavaria, Germany) thermogravimetric analyzer. The samples were heated from room temperature to 750 ^oC at a rate of 10 ^oC/min under nitrogen atmosphere. Zeta potential and dynamic light scattering (DLS) measurements were conducted using a Malvern Zetasizer Nano ZS model ZEN3600 (Worcestershire, UK) equipped with a standard 633 nm laser. Transmission electron microscopy (TEM) was performed with a JEOL 2010F analytical electron microscope (JEOL, Tokyo, Japan) operating at 200 kV. TEM samples were prepared by depositing a dilute particle suspension (5 μL) onto a carbon-

coated copper grid and air-dried before measurements. The Fe concentration of the NPs in aqueous solution was analyzed using a Leeman Prodigy inductively coupled plasma-atomic emission spectroscopy (ICP-AES) (Hudson, NH). T_1 relaxometry was performed by a 0.5 T NMI20-Analyst NMR Analyzing and Imaging system (Shanghai NIUMAG Corporation, Shanghai, China). The samples were diluted in water with an Fe concentration in a range of 0.1-1.6 mM. The instrumental parameters were set at point resolution of 156 mm × 156 mm, section thickness of 0.5 mm, TR of 400 ms, TE of 20 ms, and number of excitation of 1. The T_1 relaxivity was calculated by linear fitting the inverse T_1 relaxation time ($1/T_1$) as a function of Fe concentration.

Cytotoxicity assay and cell morphology observation

The cytotoxicity of the Fe_3O_4-*m*PEG and Fe_3O_4-PEG-RGD NPs was evaluated by MTT viability assay of U87MG cells. The cells were seeded into a 96-well plate with a density of 1×10^4 per well and incubated in regular DMEM supplemented with 10% heat-inactivated FBS, 100 U/mL penicillin, and 100 μg/mL streptomycin for 24 h. Afterwards, the medium was replaced with fresh medium containing the Fe_3O_4-*m*PEG or the Fe_3O_4-PEG-RGD NPs at different Fe concentrations. After 24 h incubation at 37 °C and 5% CO_2, MTT (20 μL, 5 mg/mL) in PBS was added to each well and the cells were incubated for another 4 h under regular culture conditions. The medium was then carefully removed, and DMSO (200 μL) was added to each well to dissolve the formed formazan crystals. The absorbance at 570 nm in each well was measured using a Thermo Scientific Multiskan MK3 ELISA reader (Thermo Scientific, Hudson, NH). Mean and standard deviation for the triplicate wells were reported.

After treatment with the Fe_3O_4-*m*PEG or Fe_3O_4-PEG-RGD NPs at different Fe concentrations (0-100 μg/mL) for 24 h, the cell morphology was observed using a Leica DM IL LED inverted phase contrast microscope with a magnification of 200 × for each sample.

Hemolysis assay

Fresh human blood stabilized with EDTA was kindly supplied by Shanghai General Hospital (Shanghai, China) and used with the permission by the ethical committee of Shanghai General Hospital. Human red blood cells (HRBCs) were obtained and hemolysis assay was performed according to the literature.[28, 30, 35, 36] Both the Fe_3O_4-*m*PEG and Fe_3O_4-PEG-RGD NPs at an Fe concentration range of 0-80 μg/mL were tested.

Cellular uptake

The specific uptake of the Fe_3O_4-PEG-RGD NPs by U87MG cells was confirmed by ICP-AES analysis of the cells treated with the particles for 4 h. In brief, U87MG cells were seeded in 12-well plates at a density of 2×10^5 cells per well in 1 mL DMEM and incubated at 37 °C and 5% CO_2. After overnight incubation to bring the cells to confluence, the medium was replaced with 1 mL fresh medium containing PBS (control), and the Fe_3O_4-*m*PEG or Fe_3O_4-PEG-RGD NPs at different Fe concentrations (20, 40, 60, 80, and 100 μg/mL, respectively). After 4 h incubation, the cells were washed 3 times with PBS, trypsinized, centrifugated, and resuspended in 1 mL PBS to count the number of cells per well before digested by aqua regia solution. Then, ICP-AES analysis was used to quantify the uptake of the Fe_3O_4-*m*PEG or Fe_3O_4-PEG-RGD NPs by U87MG cells. For comparison, normal L929 cells were also treated under similar experimental conditions.

To further qualitatively confirm the specific cellular uptake of the Fe_3O_4-PEG-RGD NPs, Prussian blue staining was employed. Similar to the ICP-AES analysis, U87MG cells were treated with the Fe_3O_4-*m*PEG or Fe_3O_4-PEG-RGD NPs for 4 h. The cells were then washed 3 times with PBS, fixed with 2.5% glutaraldehyde solution, stained with Prussian blue solution, and observed by phase contrast microscopy.

***In vitro* MR imaging of U87MG cells**

U87MG cells were seeded in a 6-well plate at a density of 3×10^6 cells per well in 2 mL DMEM and incubated at 37 °C and 5% CO_2. After overnight culture to bring the cells to confluence, the medium was replaced with 2 mL fresh medium containing the Fe_3O_4-*m*PEG or Fe_3O_4-PEG-RGD NPs at different Fe concentrations (5, 10, 25, 50, and 100 μg/mL, respectively), and then the cells were incubated at 37 °C and 5% CO_2 for 6 h. After that, the cells were washed with PBS for 5 times, trypsinized, centrifuged, and resuspended in 1 mL PBS in 2-mL Eppendorf tubes before MR imaging. T_1-positive MR imaging of the cell suspension was performed by a 0.5 T NMI20-Analyst NMR Analyzing and Imaging system using a wrist receiver coil with a sequence of inversion recovery (TR = 400 ms, TE = 20 ms, point resolution = 128 mm × 128 mm, section thickness = 0.5 mm, and number of excitation = 1).

***In vivo* MR imaging of xenografted U87MG tumor model**

Animal experiments were carried out according to protocols approved by the institutional committee for animal care, and also in accordance with the policy of the National Ministry of Health. Male 4 to 6-week-old BALB/c nude mice (15-20 g, Shanghai Slac Laboratory Animal Center, Shanghai, China) were subcutaneously injected with 5×10^6 cells/mouse in the left back. When the tumor nodules reached a volume of about 250 mm^3 at approximately 4 weeks postinjection, the mice were anesthetized by intraperitoneal injection of pentobarbital sodium (40 mg/kg), and then the Fe_3O_4-*m*PEG or Fe_3O_4-PEG-RGD NPs (dispersed in 0.3 mL PBS) were intravenously delivered into the tumor-bearing mice *via* the tail vein (450 μg Fe per mouse). For MR imaging, a 1.5 T GE Discovery MR750 scanner with an animal coil suitable for mouse imaging (Magtron Inc., Shanghai, China) was used with an FSE sequence (slice thickness = 1.8 mm, TR = 600 ms, TE = 11.7 ms, FOV = 3 × 3 cm, and point resolution = 128 × 256). For each animal, two dimensional (2D) spin-echo T_1-weighted MR images were obtained before and at 15, 45, 60, 75, 90, 120, 150, and 180 min postinjection of the particles.

***In vivo* biodistribution**

The tumor-bearing mice after MR scanning were euthanized at 12 h postinjection and the heart, liver, spleen, lung, kidney, and tumor were extracted and weighed. The organs were then cut into 1-2 mm^2 pieces and digested by aqua regia solution (nitric acid/hydrochloric acid, v/v = 1:3) for 24 h. Then, the Fe content in different organ pieces was quantified by ICP-AES. For comparison, the mice without injection and the mice injected with the nontargeted Fe_3O_4-*m*PEG NPs were used as controls.

Statistical analysis

One-way ANOVA statistical analysis was performed to evaluate the significance of the experimental data. A p value of 0.05 was selected as the level of significance, and the data were indicated with (*) for $p < 0.05$, (**) for $p < 0.01$, and (***) for $p < 0.001$, respectively.

Results and discussion

Synthesis and characterization of the Fe_3O_4-PEG-RGD NPs

Via a similar solvothermal route,[34] citrate-stabilized Fe_3O_4 NPs with a size of 2.8 nm were synthesized for subsequent modification with *m*PEG-NH_2 or PEGylated RGD with one end of amine group through EDC coupling. To form the PEGylated RGD, thiolated RGD was reacted with Mal-PEG-NH_2 through thiol-maleimide coupling. The formed RGD-PEG-NH_2 was characterized by ^{1}H NMR (Figure S1, electronic supplementary information, ESI). Through NMR integration, the number of RGD attached to each PEG was estimated to be 0.5.

Zeta potential measurements were carried out to confirm the successful surface modification of the Fe_3O_4 NPs (Table S1, ESI). The pristine citrate-stabilized Fe_3O_4 NPs have a quite negative surface potential of -39.7 mV due to the citrate stabilization. Subsequent reaction of *m*PEG-NH_2 or RGD-PEG-NH_2 significantly increases the surface potential of the particles, and the surface potentials of the Fe_3O_4-*m*PEG and Fe_3O_4-PEG-RGD NPs were measured to be -8.8 and -10.1 mV, respectively. The hydrodynamic size of the Fe_3O_4 NPs before and after surface modification was also analyzed (Table S1, ESI). It can be seen that the hydrodynamic sizes of the Fe_3O_4-*m*PEG and Fe_3O_4-PEG-RGD NPs are 168.7 nm and 212.5 nm, respectively. The increased hydrodynamic size of the NPs compared to the pristine citrate-stabilized Fe_3O_4 NPs should be attributed to the surface modification process, likely resulting in the increased tendency of certain degree of aggregation in aqueous solution. It should be notified that both Fe_3O_4-*m*PEG and Fe_3O_4-PEG-RGD NPs are quite stable in water and their hydrodynamic sizes do not have appreciable changes after at least 7 days' continuous monitoring (Figure S2, ESI). Meanwhile, both particles are stable in water, PBS, and cell culture medium and no precipitation occurs for at least 14 days (Figure S3, ESI), demonstrating the good colloidal stability of these particles.

The morphology and size of the Fe_3O_4-*m*PEG and Fe_3O_4-PEG-RGD NPs were characterized by TEM (Figure 2). Both particles display a spherical or quasi-spherical shape with a quite uniform size distribution. The mean diameter of the Fe_3O_4-*m*PEG and Fe_3O_4-PEG-RGD NPs was measured to be 2.7 ± 0.2 nm, similar to that of the pristine citrate-stabilized Fe_3O_4 NPs.[34] This suggests that the size and morphology of the particles do not have any appreciable changes after the further PEGylation modification step. It is interesting to note that the measured sizes of the Fe_3O_4-*m*PEG and Fe_3O_4-PEG-RGD NPs are much smaller than those of the respective particles measured by DLS. This should be due to the fact that TEM measures the size of the single Fe_3O_4 core particles, where DLS measures the size of large aggregates or clusters of particles in aqueous solution that may consist of many single Fe_3O_4 NPs, in agreement with the literature.[31]

TGA was performed in order to quantitatively analyze the amount of *m*PEG or PEG-RGD conjugated onto the surface of Fe_3O_4 NPs (Figure 3). It is clear that the pristine Fe_3O_4 NPs show a weight loss of 34.4% due to the presence of citrate on the particle surface. After subsequent modification with the *m*PEG or PEG-RGD, the weight loss of Fe_3O_4-*m*PEG and Fe_3O_4-PEG-RGD NPs were evaluated to be 41.1% and 44.7%, respectively. Consequently, by subtracting the weight loss of the Fe_3O_4 NPs (34.4%), we were able to calculate the loading percentages of the *m*PEG (for nontargeted particles) and PEG-RGD (for targeted particles) on the surface of the Fe_3O_4 NPs to be 6.7% and 10.3%, respectively.

T_1 relaxometry

Fe_3O_4 NPs are known to be used as T_2 negative MR contrast agents, which is able to decrease the MR signal intensity. In this study, in contrast to other previous studies,[27, 28, 36, 37] we synthesized ultrasmall Fe_3O_4-PEG-RGD NPs and tested the potential to use them as T_1 positive MR contrast agents. From the T_1-weighted MR images (Figure 4a), it is clear that both the Fe_3O_4-*m*PEG and Fe_3O_4-PEG-RGD NPs display increased MR signal intensity with the Fe concentration. By plotting the relaxation rate ($1/T_1$) as a function of Fe concentration, the r_1 of the Fe_3O_4-*m*PEG and Fe_3O_4-PEG-RGD NPs was calculated to be 1.15 and 1.37 $mM^{-1}s^{-1}$, respectively (Figure 4b). Taken together, the T_1-weighted MR images and T_1 relaxometry data suggest that the formed PEGylated Fe_3O_4 NPs could be used as potential T_1-weighted positive contrast agents for MR imaging applications.

Cytocompatibility assay

Before the use of the Fe_3O_4-PEG-RGD NPs for *in vitro* or *in vivo* MR imaging applications, the cytotoxicity of the particles was evaluated by MTT cell viability assay (Figure 5). We can clearly see that the viability of U87MG cells treated with either the targeted or nontargeted NPs slightly decreases with the Fe concentration (from 5 to 100 μg/mL) when compared with the PBS control. However, at the tested highest Fe concentration (100 μg/mL), the U87MG cells treated with either the Fe_3O_4-*m*PEG or the Fe_3O_4-PEG-RGD NPs display a quite high viability of 80.0%. These results indicate that both the Fe_3O_4-*m*PEG and Fe_3O_4-PEG-RGD NPs have good cytocompatibility in the studied concentration range.

The cytocompatibility of the PEGylated Fe_3O_4 NPs was further confirmed by observation of the morphology of U87MG cells treated with both targeted and nontargeted Fe_3O_4 NPs (Figure S4, ESI). Compared with the PBS control, the morphology of U87MG cells treated with both particles at the studied Fe concentrations (5-100 μg/mL) do not display any appreciable morphological changes. These results corroborate the MTT assay data, confirming the good cytocompatibility of both the Fe_3O_4-*m*PEG and the Fe_3O_4-PEG-RGD NPs.

Hemolysis assay

Hemocompatibility represents a critical concern for the development of contrast agents for *in vivo* biomedical applications. We evaluated the hemocompatibility of both the Fe_3O_4-*m*PEG and the Fe_3O_4-PEG-RGD NPs using hemolytic assay (Figure S5, ESI). Clearly, no hemolytic effect is observed for HRBCs treated with both NPs with an Fe concentration up to 80 μg/mL (Figure S5, right panel). The hemolytic percentages for

both NPs at different Fe concentrations (10-80 μg/mL) are less than the threshold value of 5%[38] (Figure S5, left panel). These studies indicate that both NPs have an excellent hemocompatibility in the studied concentration range.

Specific cellular uptake of the Fe_3O_4-PEG-RGD NPs

ICP-AES was used to evaluate the cellular uptake of the Fe_3O_4-PEG-RGD NPs by $\alpha_v\beta_3$ integrin-overexpressing U87MG cells (Figure 6). Normal mouse fibroblast cells without expression of $\alpha_v\beta_3$ integrin (L929 cells) were also tested for comparison (Figure S6, ESI). It can be seen that the U87MG cells display increased Fe uptake with the Fe concentration for both the Fe_3O_4-*m*PEG and Fe_3O_4-PEG-RGD NPs. However, at the same Fe concentration, the uptake of the targeted Fe_3O_4-PEG-RGD NPs by U87MG cells is much higher than that of the nontargeted Fe_3O_4-*m*PEG NPs ($p < 0.001$). In contrast to the $\alpha_v\beta_3$ integrin-overexpressing U87MG cells, at the same Fe concentration, the uptake of the Fe_3O_4-*m*PEG and the Fe_3O_4-PEG-RGD NPs in the control L929 cells do not show obvious difference. It should be noted that the Fe concentration-dependent nonspecific cellular uptake of the Fe_3O_4-*m*PEG NPs by U87MG cells and the Fe_3O_4-PEG-RGD or Fe_3O_4-*m*PEG NPs by L929 cells may be attributed to two distinct mechanisms (phagocytosis and diffusion through cell walls). And the large hydrodynamic size of both particles seems not to impact their nonspecific cellular uptake, in agreement with the literature.[22, 33, 37]

The specific cellular uptake of the Fe_3O_4-PEG-RGD by U87MG cells was further qualitatively confirmed by Prussian blue staining (Figure S7, ESI). It is clear that U87MG cells treated with the Fe_3O_4-PEG-RGD NPs display much more significant blue staining than those treated with the Fe_3O_4-*m*PEG NPs at the same Fe concentrations. In contrast, control cells treated with PBS do not display such blue staining. The Prussian blue staining results corroborate the quantitative ICP-AES data, demonstrating the role played by RGD-mediated targeting, in agreement with the literature.[39]

Targeted T_1-weighted positive MR imaging of cancer cells *in vitro*

Next, we explored the potential to use the Fe_3O_4-*m*PEG-RGD NPs as a nanoprobe for T_1-weighted positive MR imaging of cancer cells *in vitro* (Figure 7). Both the Fe_3O_4-*m*PEG and Fe_3O_4-PEG-RGD NPs are able to induce T_1-positive MR contrast enhancement of U87MG cells with the Fe concentration. Additionally, at the same Fe concentration, the MR signal intensity of the U87MG cells treated with the Fe_3O_4-PEG-RGD NPs is much higher than that of the same cells treated with the Fe_3O_4-*m*PEG NPs without RGD (Figure 7a). By plotting the T_1 MR signal to noise ratio (SNR) of the U87MG cells treated with the Fe_3O_4-*m*PEG or Fe_3O_4-PEG-RGD NPs as a function of Fe concentration (Figure 7b), it can be clearly observed that for both particles, the MR SNR increases with the Fe concentration. Notably, the MR SNR of cells treated with the Fe_3O_4-PEG-RGD NPs is significantly higher than that treated with the Fe_3O_4-*m*PEG NPs at the same Fe concentration ($p < 0.05$). This suggests that the Fe_3O_4-PEG-RGD NPs are able to be used as a nanoprobe for specific T_1-positive MR imaging of $\alpha_v\beta_3$ integrin-overexpressing cancer cells *in vitro*.

Targeted T_1-weighted positive MR imaging of xenografted U87MG tumor model *in vivo*

The potential to use the Fe_3O_4-PEG-RGD NPs as a nanoprobe for targeted T_1-weighted MR imaging of tumors *in vivo* was next investigated (Figure 8). Clearly, intravenous injection of both targeted and nontargeted NPs induces MR contrast enhancement of the U87MG tumors (Figure 8a). At 45 min postinjection, both particles are able to afford the tumor region with the maximum MR contrast enhancement likely due to the maximum accumulation of the NPs within the tumor region. The gradual decrease of MR signal intensity after 45 min postinjection should be due to the fact that the particles have undergone a metabolism process, leading to gradually decreased accumulation in the tumors. Only a slight increase in MR signal intensity has been observed in the nontargeted group in comparison to the targeted group at the same time points. The quantitative tumor MR SNR data show that at the same time point, the tumor MR SNR treated with the Fe_3O_4-PEG-RGD NPs is significantly higher than that treated with the nontargeted Fe_3O_4-*m*PEG NPs ($p < 0.001$, Figure 8b). Taken together, these MR imaging results and the MR SNR data suggest that the Fe_3O_4-PEG-RGD NPs are able to be used as a nanoprobe for targeted T_1-weighted positive MR imaging of tumors *in vivo* thanks to the RGD-mediated active targeting pathway.

***In vivo* biodistribution**

For further *in vivo* MR imaging applications, it is important to investigate the biodistribution behavior of the Fe_3O_4-PEG-RGD NPs. ICP-AES data reveal that the Fe concentration in all the organs and tumor tissue after injection of the Fe_3O_4-*m*PEG or Fe_3O_4-PEG-RGD NPs is much higher than that of the control mice without injection (Figure 9). A significant uptake in the liver and spleen occurs, while only a relatively small amount of Fe is uptaken in other organs (e.g., heart and kidney) and the tumor tissue. Clearly, the Fe biodistribution data suggest that the PEGylation modification of the Fe_3O_4 NPs allows a portion of particles to escape from the reticuloendothelial system (RES) and to deliver to the tumor tissue for effective tumor MR imaging. Importantly, the Fe concentration in the tumors of the mice treated with the targeted Fe_3O_4-PEG-RGD NPs is much higher than that treated with the nontargeted Fe_3O_4-*m*PEG NPs ($P < 0.01$). These results fully illustrates the important RGD targeting role, allowing for effective delivery of the NPs to tumors, consequently allowing for effective targeted MR imaging of tumors.

Conclusions

In summary, we developed a convenient approach to preparing RGD-functionalized ultrasmall Fe_3O_4 NPs for targeted T_1-weighted positive MR imaging of tumors *in vivo*. Using simple solvothermal decomposition technique and PEGylation conjugation chemistry, RGD-functionalized ultrasmall Fe_3O_4 NPs with a size of 2.7 nm can be prepared to have good water dispersibility, colloidal stability, and cytocompatibility and hemocompatibility in the studied Fe concentration range. Owing to the role played by RGD-mediated targeting and the inherent good r_1 relaxivity, the developed Fe_3O_4-PEG-RGD NPs are able to be used as a nanoprobe for targeted T_1-weighted positive MR

imaging of $\alpha_v\beta_3$ integrin-overexpressing glioma cells *in vitro* and the xenografted tumor model *in vivo*. Taking into consideration of the possibility to functionalize citrate-stabilized Fe_3O_4 NPs with other targeting ligands (e.g., antibodies, sugars, and other peptides) and drugs, ultrasmall Fe_3O_4 NPs may be developed as new multifunctional theranostic nanoplatforms for different biomedical applications.

Acknowledgements

This research is financially supported by the National Natural Science Foundation of China (21273032 and 81371623), the Sino-German Center for Research Promotion (GZ899), and the Program for Professor of Special Appointment (Eastern Scholar) at Shanghai Institutions of Higher Learning. M. Shen thanks the Fundamental Research Funds for the Central Universities. Y. Luo thanks the Innovation Funds of Donghua University Doctorate Dissertation of Excellence (15D310509).

Notes and references

[a] *College of Chemistry, Chemical Engineering and Biotechnology, Donghua University, Shanghai 201620, People's Republic of China E-mail: xshi@dhu.edu.cn (X. Shi) and mwshen@dhu.edu.cn (M. Shen)*
[b] *Department of Radiology, Shanghai General Hospital, Shanghai Jiaotong University, School of Medicine, Shanghai 200080, People's Republic of China. E-mail: guixiangzhang@sina.com*
[c] *Université Paris Descartes, PRES Sorbonne Paris Cité, CNRS UMR 860, Laboratoire de Chimie et de Biochimie pharmacologiques et toxicologique, 45, rue des Saints Pères, 75006 Paris, France*
[1] *Yu Luo and Jia Yang contributed equally to this work.*

† **Electronic supplementary information (ESI) available**: additional experimental results.

1. M. R. Ramaswamy, G. Chaljub, O. Esch, D. D. Fanning and E. vanSonnenberg, *Am. J. Roentgenol.*, 2000, **174**, 617-622.
2. R. T. Heelan, B. E. Demas, J. F. Caravelli, N. Martini, M. S. Bains, P. M. McCormack, M. Burt, D. M. Panicek and A. Mitzner, *Radiology*, 1989, **170**, 637-641.
3. S. Aime, C. Cabella, S. Colombatto, S. Geninatti Crich, E. Gianolio and F. Maggioni, *J. Magn. Reson. Imaging*, 2002, **16**, 394-406.
4. X. Hu and D. G. Norris, *Annu. Rev. Biomed. Eng.*, 2004, **6**, 157-184.
5. P. Marckmann, L. Skov, K. Rossen, A. Dupont, M. B. Damholt, J. G. Heaf and H. S. Thomsen, *J. Am. Soc. Nephrol.* , 2006, **17**, 2359-2362.
6. M. Tan, Z. Ye, E.-K. Jeong, X. Wu, D. L. Parker and Z.-R. Lu, *Bioconjugate Chem.*, 2011, **22**, 931-937.
7. C. Thakral, J. Alhariri and J. L. Abraham, *Contrast Media Mol. Imaging* 2007, **2**, 199-205.
8. M. A. Sieber, P. Lengsfeld, J. Walter, H. Schirmer, T. Frenzel, F. Siegmund, H. J. Weinmann and H. Pietsch, *J. Magn. Reson. Imaging* 2008, **27**, 955-962.
9. A. G. Roca, J. F. Marco, M. P. Morales and C. J. Serna, *J. Phys. Chem. C* 2007, **111**, 18577-18584.
10. Y. Jun, J. H. Lee and J. Cheon, *Angew. Chem., Int. Ed.*, 2008, **47**, 5122-5135.
11. R. Kodama, *J. Magn. Magn. Mater.* , 1999, **200**, 359-372.
12. G. Wang, X. Zhang, A. Skallberg, Y. Liu, Z. Hu, X. Mei and K. Uvdal, *Nanoscale*, 2014, **6**, 2953-2963.
13. L. Zeng, W. Ren, J. Zheng, P. Cui and A. Wu, *Phys. Chem. Chem. Phys.*, 2012, **14**, 2631-2636.
14. U. I. Tromsdorf, O. T. Bruns, S. C. Salmen, U. Beisiegel and H. Weller, *Nano Lett.* , 2009, **9**, 4434-4440.
15. E. Taboada, E. Rodríguez, A. Roig, J. Oró, A. Roch and R. N. Muller, *Langmuir*, 2007, **23**, 4583-4588.
16. J. Xie, K. Chen, H. Y. Lee, C. Xu, A. R. Hsu, S. Peng, X. Chen and S. Sun, *J. Am. Chem. Soc.*, 2008, **130**, 7542-7543.
17. B. H. Kim, N. Lee, H. Kim, K. An, Y. I. Park, Y. Choi, K. Shin, Y. Lee, S. G. Kwon and H. B. Na, *J. Am. Chem. Soc.*, 2011, **133**, 12624-12631.
18. W. Y. William, E. Chang, C. M. Sayes, R. Drezek and V. L. Colvin, *Nanotechnology*, 2006, **17**, 4483-4487.
19. J. A. Barreto, W. O'Malley, M. Kubeil, B. Graham, H. Stephan and L. Spiccia, *Adv. Mater.*, 2011, **23**, 18-40.
20. H. Maeda, *Bioconjugate Chem.*, 2010, **21**, 797-802.
21. C. Minelli, S. B. Lowe and M. M. Stevens, *Small*, 2010, **6**, 2336-2357.
22. H. Wang, L. Zheng, C. Peng, R. Guo, M. Shen, X. Shi and G. Zhang, *Biomaterials*, 2011, **32**, 2979-2988.
23. L. Shen, J. Bao, D. Wang, Y. Wang, Z. Chen, L. Ren, X. Zhou, X. Ke, M. Chen and A. Yang, *Nanoscale*, 2013, **5**, 2133-2141.
24. D. Li, Q. He, Y. Yang, H. Möhwald and J. Li, *Macromolecules*, 2008, **41**, 7254-7256.
25. D. Li, C. Li, A. Wang, Q. He and J. Li, *J. Mater. Chem.*, 2010, **20**, 7782-7787.
26. D. Li, Q. He and J. Li, *Adv. Colloid Interface Sci.*, 2009, **149**, 28-38.
27. H. Cai, X. An, J. Cui, J. Li, S. Wen, K. Li, M. Shen, L. Zheng, G. Zhang and X. Shi, *ACS Appl. Mater. Interfaces*, 2013, **5**, 1722-1731.
28. J. Li, Z. L., C. H., S. W., S. M., Z. G. and S. X., *Biomaterials*, 2013, **34**, 8382-8392.
29. J. Li, Y. He, W. Sun, Y. Luo, H. Cai, Y. Pan, M. Shen, J. Xia and X. Shi, *Biomaterials*, 2014, **35**, 3666-3677.
30. J. Li, Y. Hu, J. Yang, W. Sun, H. Cai, P. Wei, Y. Sun, G. Zhang, X. Shi and M. Shen, *J. Mater. Chem. B*, 2015, DOI: 10.1039/C1035TB00849B.
31. Y. Hu, J. Li, J. Yang, P. Wei, Y. Luo, L. Ding, W. Sun, G. Zhang, X. Shi and M. Shen, *Biomater. Sci.*, 2015, **3**, 721-732.
32. X. Shi, S. H. Wang, S. D. Swanson, S. Ge, Z. Cao, M. E. Van Antwerp, K. J. Landmark and J. R. Baker, *Adv. Mater.*, 2008, **20**, 1671-1678.
33. Z. Qiao and X. Shi, *Prog. Polym. Sci.*, 2015, **44**, 1-27.
34. J. Yang, Y. Luo, Y. Xu, J. Li, Z. Zhang, H. Wang, M. Shen, X. Shi and G. Zhang, *ACS Appl. Mater. Interfaces*, 2015, **7**, 5420-5428.
35. J. Meng, Z. Z. Han, H. Kong, X. J. Qi, C. Y. Wang, S. S. Xie and H. Y. Xu, *J. Biomed. Mater. Res. Part A*, 2010, **95A**, 312-320.
36. J. Li, Y. Hu, J. Yang, P. Wei, W. Sun, M. Shen, G. Zhang and X. Shi, *Biomaterials*, 2015, **38**, 10-21.
37. J. Li, X. Shi and M. Shen, *Part. Part. Syst. Charact.*, 2014, **31**, 1223-1237.
38. S. Wang, R. Castro, X. An, C. Song, Y. Luo, M. Shen, H. Tomas, M. Zhu and X. Shi, *J. Mater. Chem.*, 2012, **22**, 23357-23367.
39. R. Shukla, E. Hill, X. Shi, J. Kim, M. C. Muniz, K. Sun and J. R. Baker, *Soft Matter*, 2008, **4**, 2160-2163.

Figure captions

Figure 1. Schematic illustration of the preparation of Fe_3O_4-PEG-RGD NPs.

Figure 2. TEM image and size distribution histogram of the Fe_3O_4-*m*PEG (a) and Fe_3O_4-PEG-RGD (b) NPs.

Figure 3. TGA curves of Fe_3O_4, Fe_3O_4-*m*PEG, and Fe_3O_4-PEG-RGD NPs.

Figure 4. T_1-weighted MR imaging of the Fe_3O_4-*m*PEG (Nontargeted) and Fe_3O_4-PEG-RGD (Targeted) NPs at the Fe concentrations of 0.05, 0.1, 0.2, 0.4, and 0.8 mM, respectively (a). (b) shows the linear fitting of $1/T_1$ of the Fe_3O_4-*m*PEG or Fe_3O_4-PEG-RGD NPs as a function of Fe concentration.

Figure 5. MTT viability assay of U87MG cells after treatment with the Fe_3O_4-*m*PEG or Fe_3O_4-PEG-RGD NPs with different Fe concentrations for 24 h. U87MG cells treated with PBS were used as control.

Figure 6. The Fe uptake in U87MG cells after the cells were treated with the Fe_3O_4-*m*PEG or Fe_3O_4-PEG-RGD NPs with different Fe concentrations for 4 h. U87MG cells treated with PBS were used as control.

Figure 7. *In vitro* T_1-weighted MR imaging (a) and MR SNR (b) of U87MG cells treated with the Fe_3O_4-*m*PEG (Nontargeted) or Fe_3O_4-PEG-RGD (Targeted) NPs at different Fe concentrations for 6 h.

Figure 8. *In vivo* T_1-weighted MR imaging (a) and MR SNR (b) of xenografted U87MG tumors after intravenous injection of Fe_3O_4-*m*PEG (Nontargeted) or Fe_3O_4-PEG-RGD (Targeted) NPs (450 μg Fe, in 0.3 mL PBS) at different time points postinjection.

Figure 9. *In vivo* biodistribution of Fe in the major organs of the mice including heart, liver, spleen, lung, kidney, and tumor at 12 h post intravenous injection of the Fe_3O_4-*m*PEG (Nontargeted) or Fe_3O_4-PEG-RGD (Targeted) NPs (450 μg Fe, in 0.3 mL PBS).

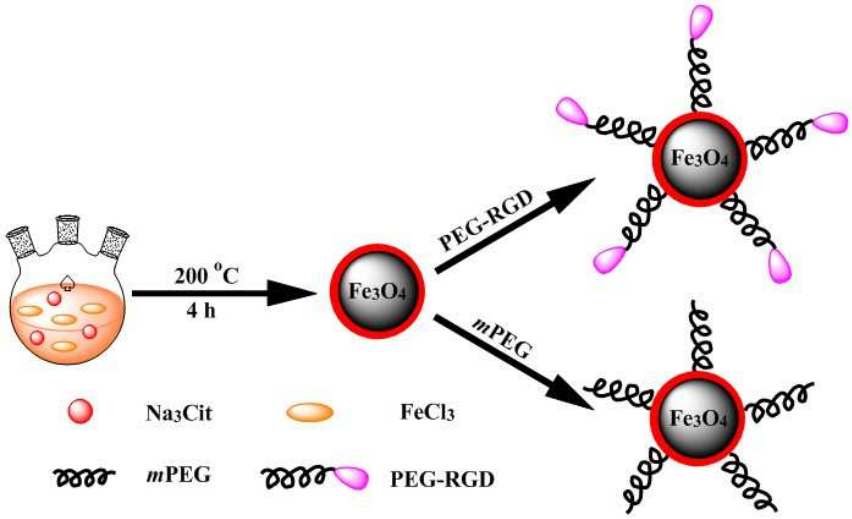

Figure 1
Luo et al.

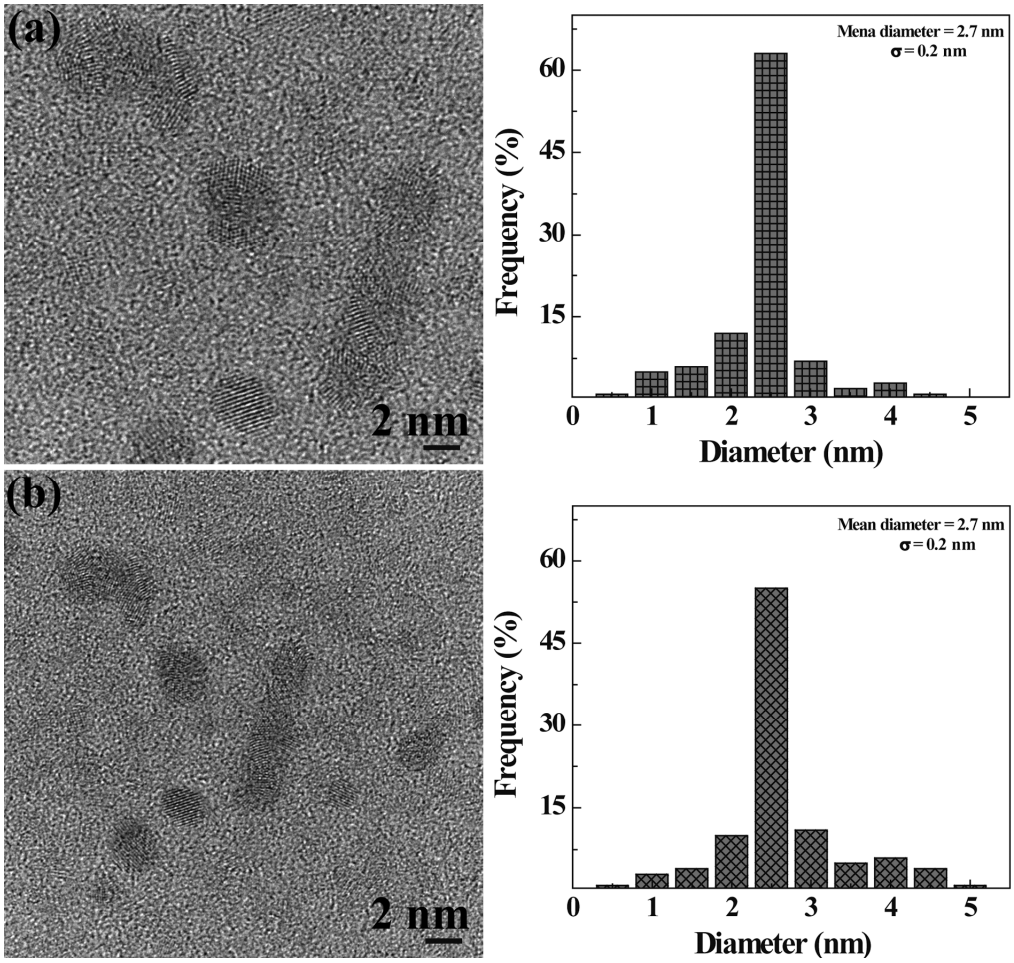

Figure 2
Luo *et al.*

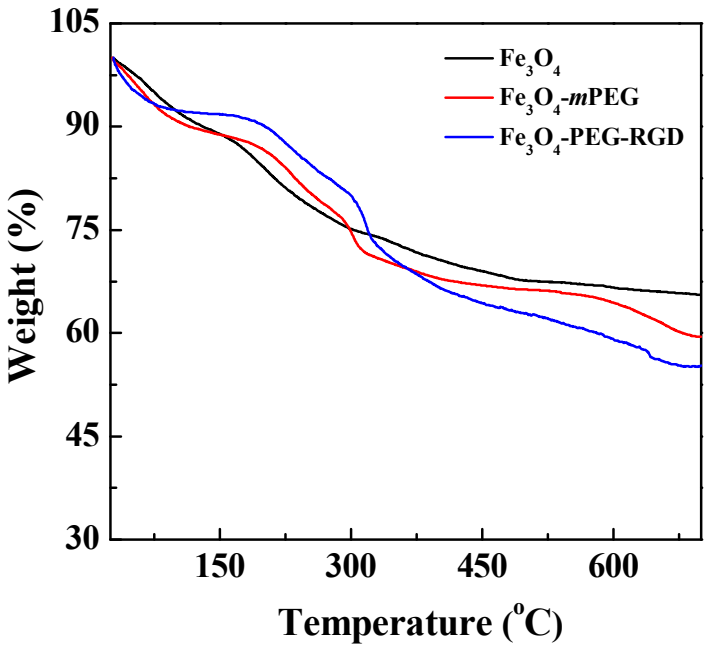

Figure 3
Luo *et al.*

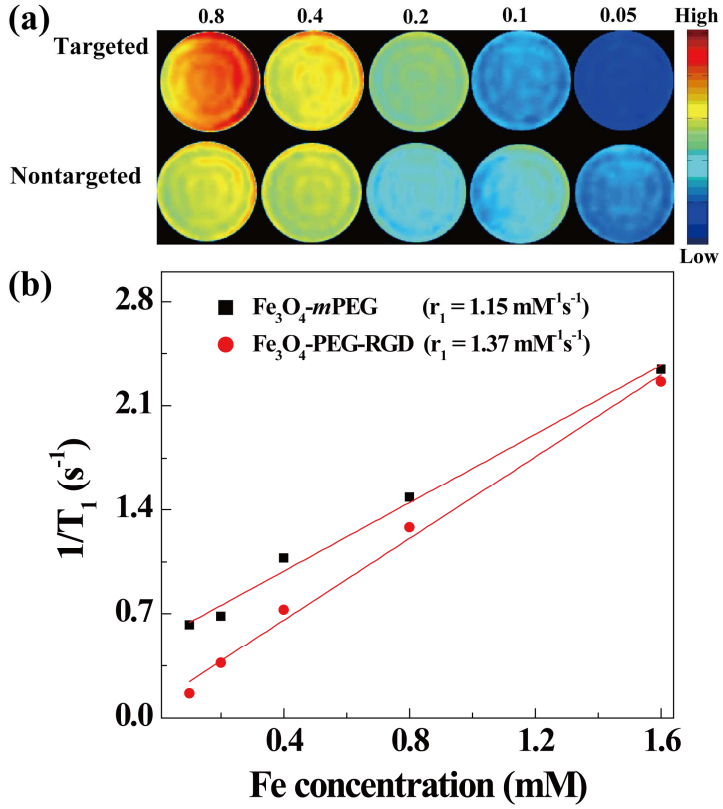

Figure 4
Luo *et al.*

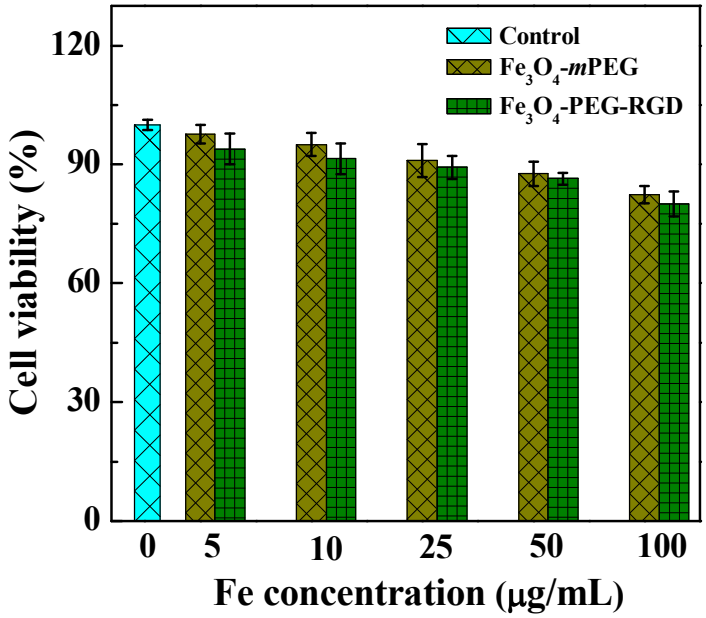

Figure 5
Luo *et al.*

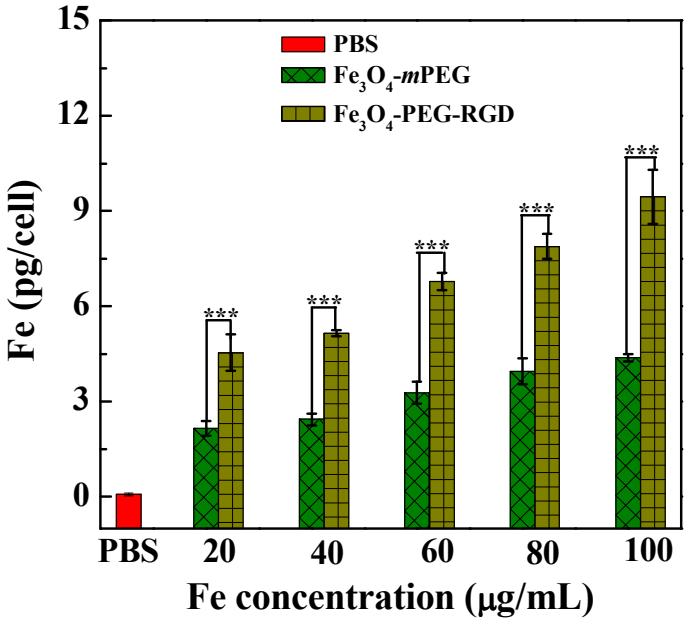

Figure 6
Luo *et al.*

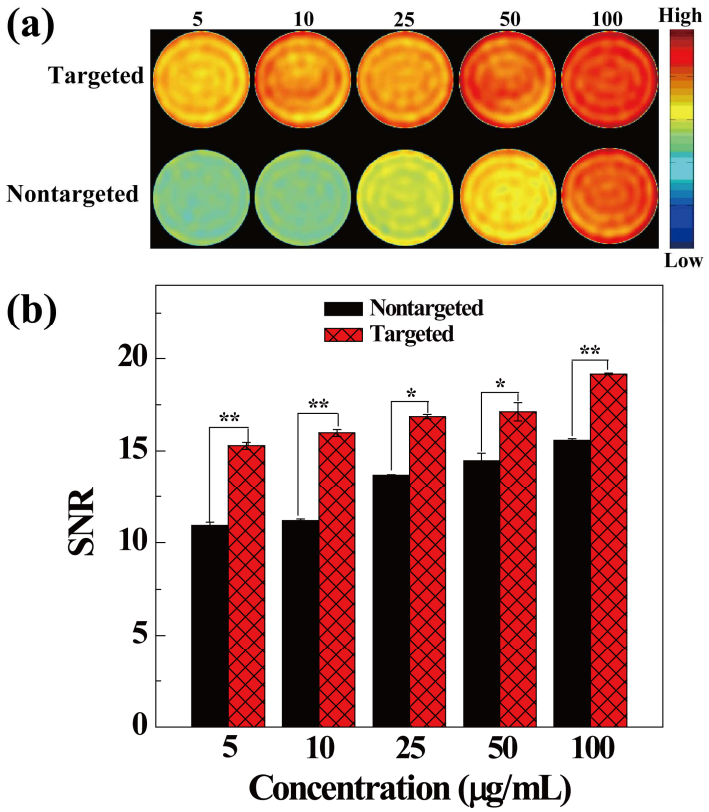

Figure 7
Luo *et al.*

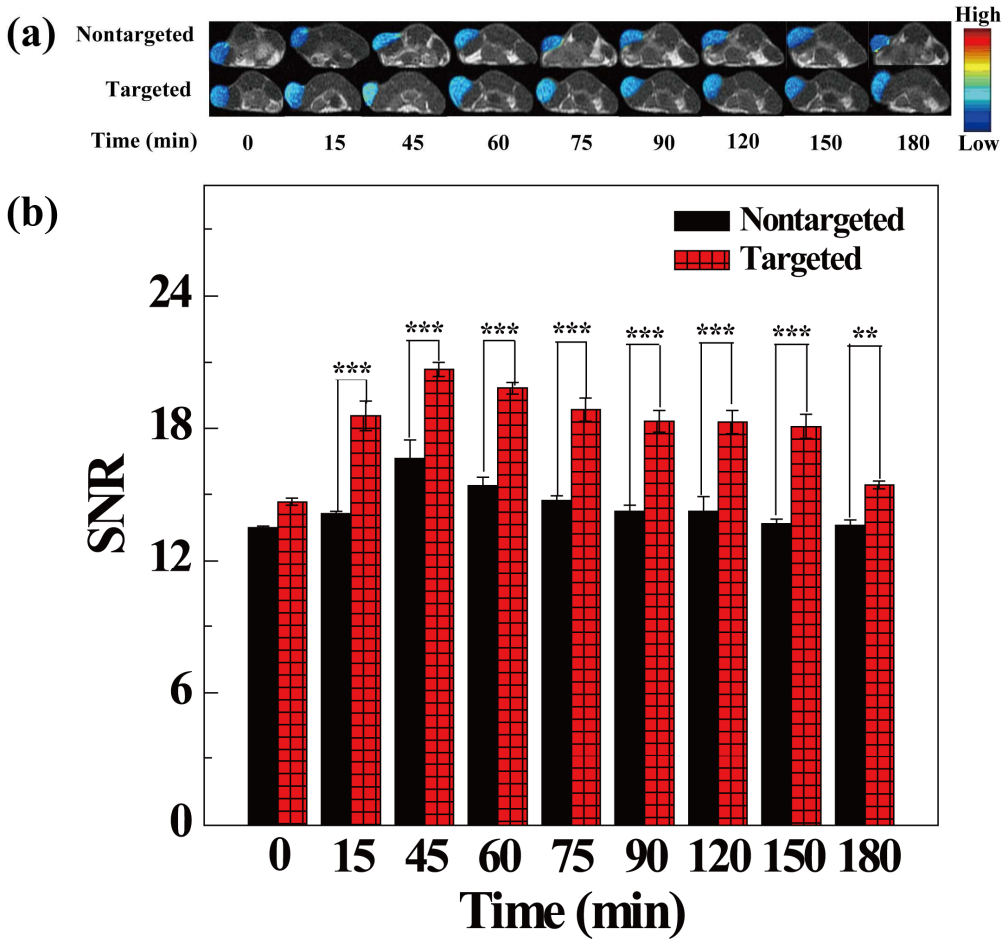

Figure 8
Luo *et al.*

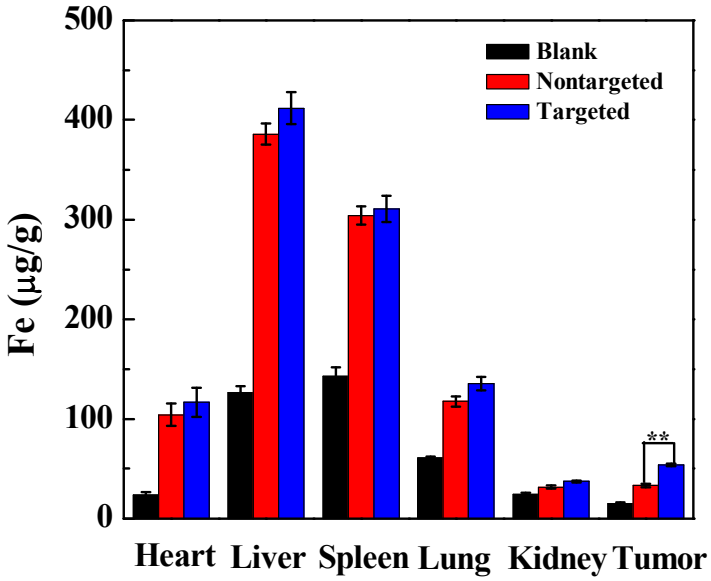

Figure 9
Luo *et al.*